Raman spectroscopy study of heavy-ion-irradiated α-SiC

INSTITUTE OF PHYSICS PUBLISHING JOURNAL OF PHYSICS: CONDENSED MATTER

J. Phys.: Condens. Matter **18** (2006) 5235–5251 doi:10.1088/0953-8984/18/22/022

Raman spectroscopy study of heavy-ion-irradiated α-SiC

S Sorieul[1], J-M Costantini[1,5], L Gosmain[2], L Thomé[3] and J-J Grob[4]

[1] CEA/Saclay, DMN/SRMA, 91191 Gif sur Yvette Cedex, France
[2] CEA/Saclay, DMN/SEMI, 91191 Gif sur Yvette Cedex, France
[3] CSNSM, CNRS/IN2P3, Université Paris Sud, 91405 Orsay Cedex, France
[4] InESS (PHASE), UMR 7163, 23 rue du Loess, BP 20, 67037 Strasbourg Cedex 2, France

E-mail: jean-marc.costantini@cea.fr

Received 15 November 2005, in final form 31 March 2006
Published 19 May 2006
Online at stacks.iop.org/JPhysCM/18/5235

Abstract

Raman spectroscopy was used to investigate the structure of ion-irradiated α-SiC single crystals at room temperature and 400 °C. Irradiations induce a decrease of the Raman line intensities related to crystalline SiC, the appearance of several new Si–C vibration bands attributed to the breakdown of the Raman selection rules, and the formation of homonuclear bonds Si–Si and C–C within the SiC network. For low doses, the overall sp^3 bond structure and the chemical order may be almost completely conserved. By contrast, the amorphous state shows a strong randomization of the Si–Si, Si–C and C–C bonds. The relative Raman intensity decreases exponentially versus increasing dose due to the absorption of the irradiated layer. The total disorder follows a sigmoidal curve, which is well fitted by the direct impact/defect stimulated model. The chemical disorder expressed as the ratio of C–C bonds to Si–C bonds increases exponentially versus the dose. A clear correlation is established between the total disorder and the chemical disorder. The increase of temperature allows the stabilization of a disordered/distorted state and a limitation of damage accumulation owing to the enhancement of the dynamic annealing.

1. Introduction

Owing to its structural, chemical and mechanical stability, silicon carbide (SiC) has been proposed for structural components in harsh environments such as a high-temperature reactor (HTR), where high-temperature and high-radiation conditions are involved. A fundamental understanding of the accumulation and recovery of irradiation damage is thus needed to improve the utilization of SiC for this technological use.

[5] Author to whom any correspondence should be addressed.

0953-8984/06/225235+17$30.00

Radiation effects induced by neutrons at high temperature were widely studied. Microstructural evolution over a large range of temperature [1–3] and swelling [1, 4, 5] were the main investigated topics. However, the results were in general limited due to the exclusive use of the TEM technique or scattered in the case, for instance [6], of the swelling at irradiation temperatures higher than 1000 °C. In the meantime, simulation of neutron damage using ions has been considered as a prominent alternative due to the limitations and difficulties generally encountered with neutron irradiations. Extensive studies were done on microstructure [7–9], amorphization [10–13], annealing processes [14–16] and recrystallization [17–21] of ion-irradiated SiC. Complementary reviews of ion irradiation were given by Wendler *et al* [13] and by Weber *et al* [12]. Nevertheless, most of the previous studies have been carried out at or below the critical temperature of amorphization T_c. Damage accumulation at higher temperatures, which involves significant defect recovery and self-clustering processes, may be more relevant to nuclear applications.

Ion-channelling methods based on Rutherford backscattering spectrometry (RBS/C) and TEM are frequently employed [22–25], whereas spectroscopic tools [26–31] which are less destructive give access to structural information. Spectroscopic techniques can also detect some complementary aspects of the transformation between the crystalline and amorphous state. Raman spectroscopy gives additional details on the composition of damaged layers and shows the appearance of chemical reordering (the formation of homonuclear bonds, which cannot be detected by IR spectroscopy) in damaged layers [26, 30, 32–35]. It also seems to be an excellent tool to monitor the disorder accumulation [36, 37].

The purpose of this paper is the investigation of the damage accumulation in ion-irradiated single crystals of SiC at room temperature and 400 °C. The structure of the irradiated layer is determined by Raman spectroscopy. Its evolution is described and discussed on the basis of the existent experimental and numerical data. The total and chemical disorders are extracted from Raman spectra and their evolutions as functions of the dose in dpa are commented. Finally, the effects of the irradiation temperature and of the ion species used for the irradiations are studied.

2. Experiments

6H- and 4H-SiC single-crystal wafers grown by the Lely method were prepared in the LETI Laboratory (CEA/Grenoble, France). The normal to the surface was around respectively 3° and 8° off the [00.1] orientation. Samples were doped with nitrogen in the range of 10^{18} cm^{-3}.

6H-SiC was irradiated with 4 MeV Au ions at room temperature and 400 °C. The temperature of 400 °C is a key value because it is well above the critical temperature of amorphization [25] but low enough to expect some radiation damage, despite the dynamic annealing induced by the increased temperature. 4H-SiC was irradiated at 400 °C with 4 MeV Xe ions. Similar conditions of irradiation were used in order to check a possible chemical effect of Au ions. The fluences were varied from 10^{12} to 10^{16} cm^{-2} and the beam current density was maintained in the range of 0.1–2 μA cm^{-2} to avoid high-dose-rate effects and excessive target heating. In order to minimize channelling effects, the normal to the sample surface was tilted by 6.5° with respect to the incident beam direction. Au-ion irradiations were performed at the ARAMIS facility (CSNSM-Orsay) and Xe-ion irradiations were done at the PHASE facility (Strasbourg). Ion fluences were converted to their equivalent doses of displacements per atom (dpa) based on the SRIM-2003 full-cascade simulations [38] and a specific density of 3.21×10^3 kg m^{-3}. The recommended threshold displacement energies [39] of 20 and 35 eV for C and Si sublattices respectively were used.

Raman scattering and confocal Raman spectra were recorded at room temperature in a backscattering geometry using a Jobin-Yvon T64000 spectrometer coupled with an Olympus

microscope that contains an X–Y–Z stage. The microscope stage could be adjusted with an accuracy of 0.5 μm along the optical axis. The 514.5 nm line of an argon ion laser was focused on a 1×1 μm^2 spot and collected through a 100$\times$ objective with a numerical aperture value of 0.9. The laser intensity was kept around 30 mW to avoid any heating of the sample. To analyse the different Si–Si, Si–C and C–C related modes, the spectra were measured in the broad spectral range between 15 and 1800 cm^{-1}.

The confocal microscope combines focused illumination with spatially filtered detection, to collect photons that originate from a diffraction-limited sample volume and reject photons that originate from outside that region. This arrangement ensures that only light coming from the focal plane entirely reaches the detector. This accounts for the confocal Raman microprobe's ability to discriminate between parts of the sample that are not at the same depth, thus allowing optical sectioning. The confocal depth resolution along the optical axis was determined using the 100 μm pinhole on a virgin 6H-SiC sample. In this experiment, the sample was slowly scanned towards the focus of the laser beam and the signal intensity of the four first-order Raman lines was measured. The average of intensities was plotted versus the scan depth z and the full width at half maximum of the resulting curve was determined corresponding to the depth resolution. With this method, we got a confocal depth resolution of 7 μm.

The fitting module of the Labspec Raman spectroscopy software (Jobin-Yvon) was used for the simulation of the Raman spectra. A Lorentzian fit is often used for crystals, arising from the finite phonon lifetime broadening, whereas a Gaussian line shape is expected for a random distribution of lifetimes in disordered materials. The irradiated layer seems to evolve from a disordered to an amorphous state. Therefore, Voigt profiles were preferentially chosen for Si–Si and Si–C vibrations in order to take into account the increasing contribution of the Gaussian shape due to the accumulation of damage. The C–C vibrations are apart from these considerations as the most widely used fit is a Breit–Wigner–Fano (BWF) line for the G band and a Lorentzian profile for the D-peak [40–42]. The BWF line has an asymmetric line shape. Since such a profile is not available in the Labspec program, the two-Gaussian fit was finally used, even though it does not provide an accurate fit of C–C bands. The signal-to-noise ratio is quite significant especially in the C–C vibration range, due to low acquisition times. The accuracy on band positions deduced from spectrum simulation is ± 5 cm^{-1}.

3. Results

3.1. Undamaged α-SiC

Group-theoretical analysis shows that the Raman-active modes of the wurtzite structure (C_{6v} symmetry for hexagonal polytypes) are the A_1, E_1 and E_2 modes. The A_1 and E_1 phonon modes are split into longitudinal (LO) and transverse (TO) optical modes. In backscattering geometry, the A_1(LO), E_1(TO) and E_2 phonons are expected to be seen in the Raman spectra. Characteristic Raman spectra of 6H- and 4H-SiC samples recorded in the same conditions are presented in figures 1(a) and (b). The major peaks in the 4H and 6H Raman spectra are identifiable from previous studies [43–46]. Their positions and corresponding assignments are summarized in table 1.

The A_1(LO) phonon line shape depends strongly on the nitrogen doping concentration in 4H-SiC [44]. Because of the high doping concentration in our sample, the peak is broadened and its intensity is low.

The high quality of samples allows the observation of several weaker peaks, the second-order Raman bands, located in the 500 and 1400–1850 cm^{-1} regions.

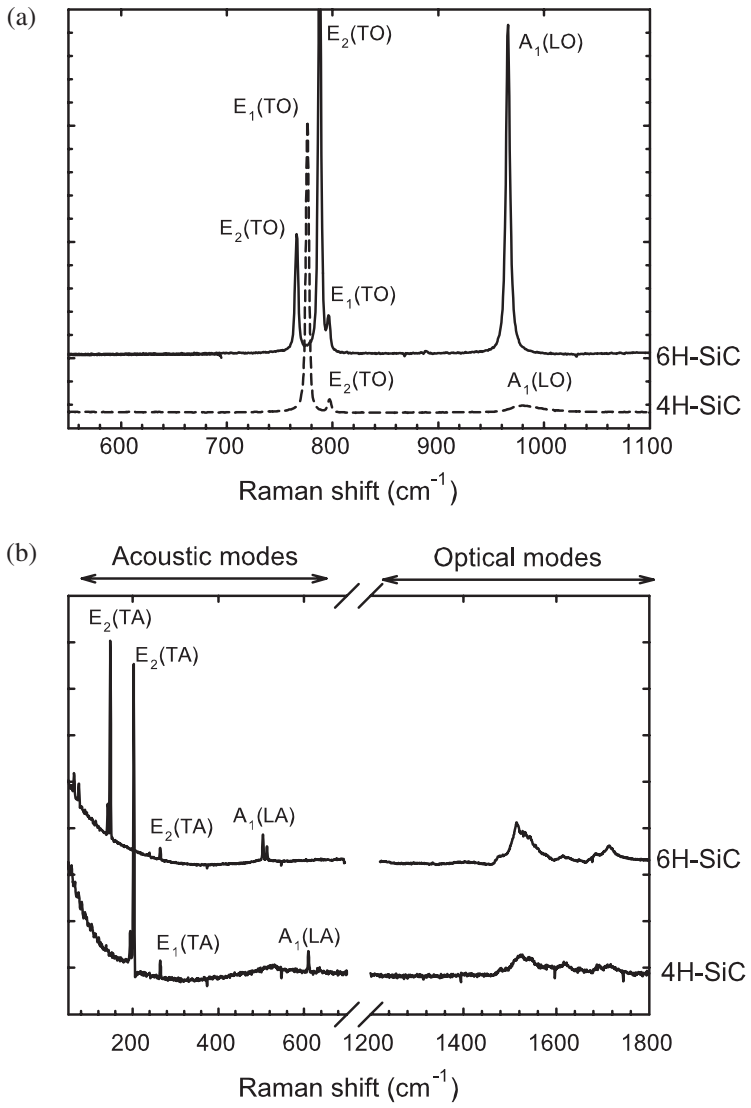

Figure 1. Raman spectra of virgin 6H- and 4H-SiC: (a) first-order and (b) second-order peaks.

3.2. Irradiated SiC

Raman spectra of Au-irradiated α-SiC at room temperature are shown in figures 2(a) and (b). Their evolution is significant of a modification of the local structure induced by irradiations. For the lowest dose (0.003 dpa), the irradiated sample spectrum is similar to the virgin one, which suggests that α-SiC is weakly damaged or is undamaged. At moderate dose (0.026 dpa), three broad bands appear around 200, 520 and 1420 cm^{-1} in addition to the first-order lines of crystalline SiC. They are characteristic [30, 34, 35] of Si–Si (200 and 520 cm^{-1}) and C–C homonuclear bonds (1420 cm^{-1}).

More than 20 bands were necessary to fit the Raman spectrum recorded for a sample irradiated at 0.026 dpa (figure 3(a)). They are associated with the vibrations of silicon (20–

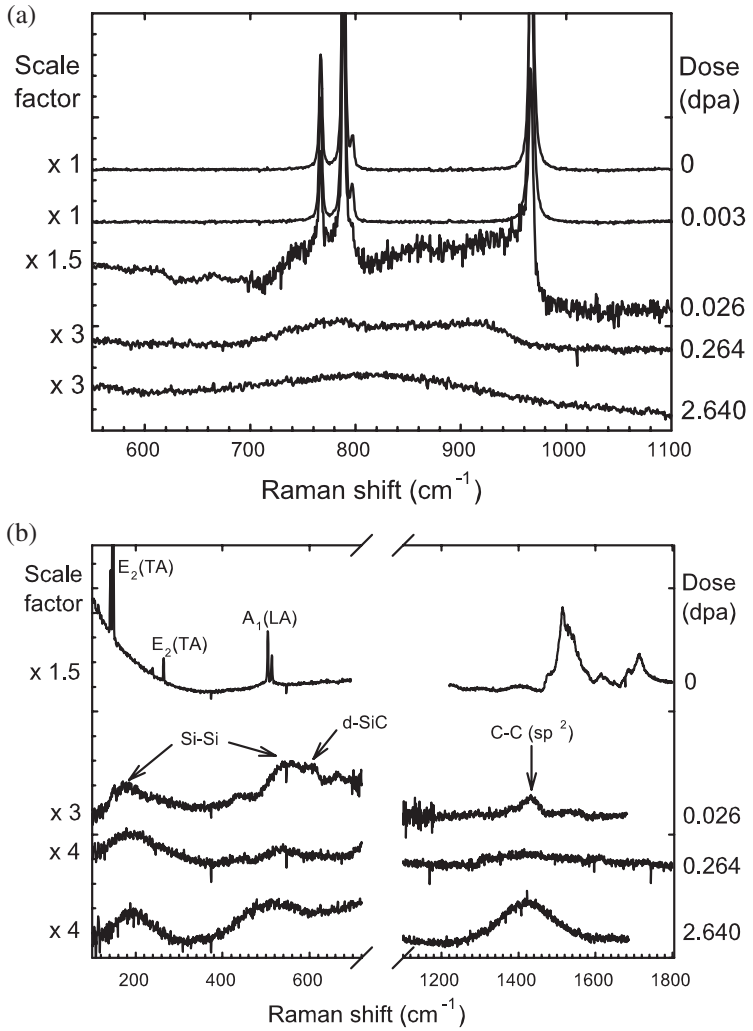

Figure 2. Raman spectra of Au-ion irradiated 6H-SiC at room temperature: (a) first-order and (b) second-order peaks.

Table 1. Frequency (in cm^{-1}) and assignment for peaks shown in figures 1(a) and (b).

6H	4H	Attribution
146, 150	196, 201	E_2(TA) [44, 46]
235, 240	264	E_1(TA) [44, 46]
266	—	E_2(TA) [44, 46]
505, 513	609	A_1(LA) [44, 46]
767, 789	776	E_2(TO) [44, 46]
797	796	E_1(TO) [44, 46]
888	—	A_1(LO) [44, 46]
967	982	A_1(LO) [44, 46]
1516, 1532, 1542	1528	Optical branch [45]
1614, 1626, 1651	1616	Optical branch [45]
1686, 1714	1692, 1710	Optical branch [45]

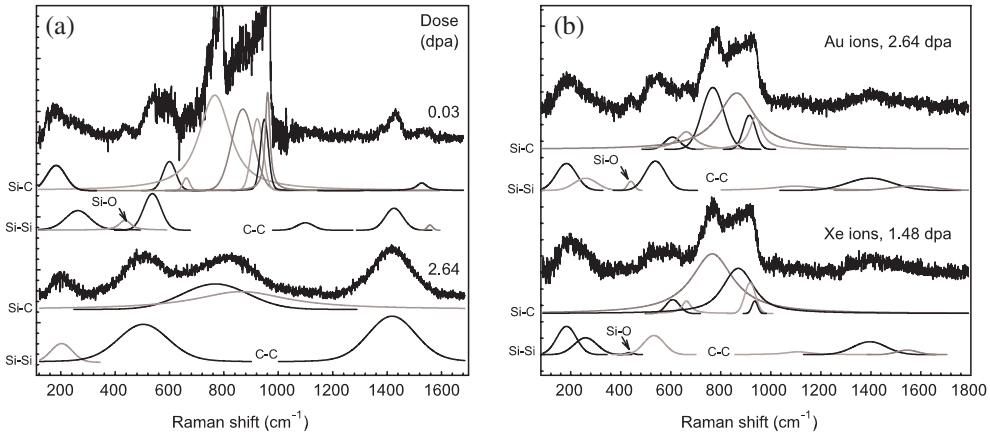

Figure 3. Curve fit of the full range spectrum for a sample irradiated (a) with Au ions at room temperature for 0.03 dpa and 2.64 dpa and (b) with Au ions at 400 °C for 2.64 dpa and with Xe ions at 400 °C for 1.48 dpa.

Table 2. Positions (in cm^{-1}) and assignments of the nine bands observed in figures 2 and 3 (am. for amorphous structure, cryst. for crystalline structure).

Si–Si vibrations		Si–C vibrations		C–C vibrations	
180–200	Cryst. Si (TA) [47–49]	148	Cryst. SiC (1st-order) [44, 46]	1080–1090	C sp^3 (?) [51, 52]
∼260	Cryst. Si (LA + LO) [47–49]	580–600 ∼660	Distorted/disordered SiC [26, 28]	1400–1420	C sp^2 (D band) [50–56]
430–440	Si–O (?) [50]	766, 789, 797, 967	Cryst. SiC (1st-order) [44, 46]	1415–1420	Am. mixed sp^2/sp^3 C [30, 34, 57]
∼500	Am. Si [47–49]	∼767 ∼870	Highly disordered or am. SiC	1560–1600	C sp^2 (G band) [50–56]
535–540	Cryst. Si (TO) [47–49]	915–920, 935–940 ∼966	Slightly disordered/distorted SiC		
		∼1530	Cryst. SiC (2nd-order) [45]		

600 cm^{-1}), silicon carbide (700–1000 cm^{-1}) and carbon (1100–1800 cm^{-1}). The assignment of the main Raman peaks is summarized in table 2. Figure 4 shows corresponding confocal spectra recorded for the same sample at various z-scan depths. For the $z = 1$ μm scan, the Raman spectrum is composed of nine bands in addition to the characteristic crystalline peaks of SiC. Their intensities decrease when the z-scan depth increases. Simultaneously, the four crystalline peaks become sharper. For a depth scan of 5 μm, the Raman spectrum is similar to that of the virgin sample. Obviously, the nine bands are related to the damaged layer and the crystal line peaks are issued from the non-irradiated part of the sample. In fact the Raman spectrum of irradiated SiC is composed of two contributions from the irradiated layer and the non-irradiated part of the sample because SiC is transparent to the laser light [26, 35]. It is also possible to identify the band around 1520 cm^{-1} as the second-order Raman lines of crystalline SiC.

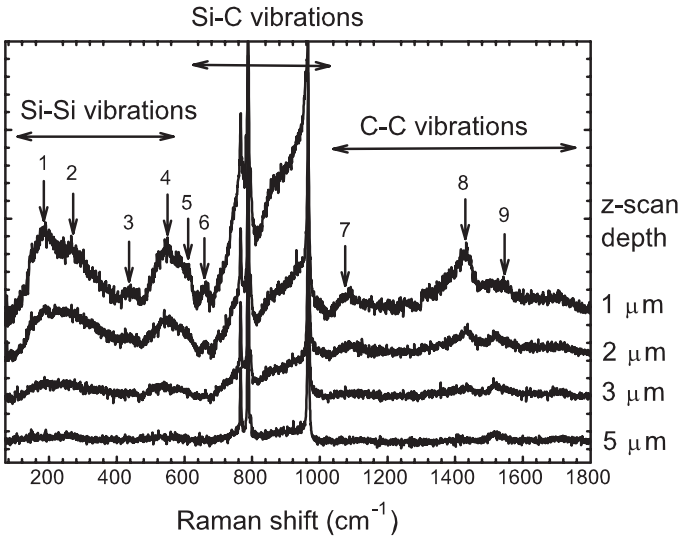

Figure 4. Confocal Raman spectra of room temperature Au-ion-irradiated α-SiC for 0.026 dpa. Acquisitions for different z-scan depths.

The increase of the dose induces a decrease of the crystalline peak intensity and an enhancement of homonuclear band intensity (figures 2(a) and (b)). The crystalline peaks completely vanish for 2.64 dpa, probably because of the increased absorption of the Raman-scattered light by the damaged layer. The crystalline peaks are not directly observed in the spectrum of the sample irradiated at 0.264 dpa, but simulation of the corresponding Raman spectrum showed that the E_2(TO) (for 6H-SiC) and E_1(TO) modes (for 4H-SiC) are still necessary to the fit. For the highest dose (2.64 dpa), only four broad bands remain at wavenumbers around 200, 500, 800 and 1420 cm^{-1}. The corresponding fitted spectrum is reported in figure 3. Only five bands are necessary to reproduce the Raman spectrum, equally distributed over the three domains of vibrations Si–Si, Si–C and C–C. The fit also puts in evidence a broadening of the bands upon irradiation. This is probably due to the amorphization of the irradiated layer that is confirmed by Rutherford backscattering and channelling (RBS/C) analysis (results not shown).

3.3. Influence of irradiation parameters: temperature and ion species

The increase of the irradiation temperature has a strong effect on the evolution of Raman spectra. A reduction of damage is noticed and the amorphization is avoided (figure 3(b)). The estimated critical temperature of amorphization [23] for 2 MeV Au-ion irradiated SiC is 500 K (∼250 °C), which is well above the temperature of study. However, irradiation at 400 °C (for 1.48 dpa) still induces important damage with the creation of homonuclear bonds (characteristic bands of Si–Si and C–C around 500 and 1400 cm^{-1}) and the disordering of the SiC network (appearance of new Si–C vibrations in the 600–900 cm^{-1} range). According to the fit, the structure of the irradiated layer is close to that obtained for 0.026 dpa at room temperature (figure 3(a)).

Recent studies of Au-ion-irradiated SiC at high temperature showed that the accumulation of disorder was considerably reduced with the rising temperature [25, 58]. On the basis on RBS/C data, Jiang *et al* [25] attributed a part of the disorder to the substitution of Si atoms

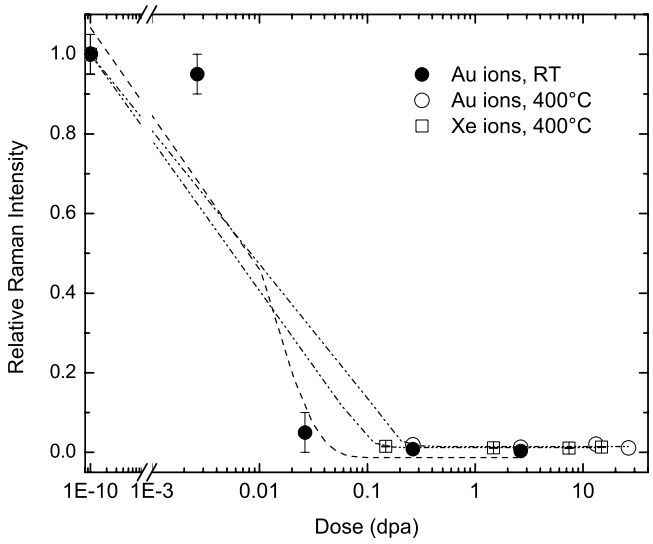

Figure 5. Relative Raman intensity (RRI) determined for Au-ion irradiations at room temperature and at 400 °C and for Xe-ion irradiations at 400 °C. Dashed (for RT irradiation) and dashed-and-dotted (for high irradiation temperature) lines represent the fit with an exponential decay.

by Au ions by analogy with the doping of silicon with Au, Ag or Pt ions [59, 60]. Such atomic substitution should have an influence on the vibrational spectrum of the material and therefore should be evidenced by Raman spectroscopy. In order to distinguish radiation effects from potential atomic substitutions on Raman spectra, Xe-ion irradiations were done at 400 °C. A simulation of the Raman spectrum of Xe-ion-irradiated α-SiC for 1.48 dpa is presented and compared with the Raman spectrum recorded for an Au-ion irradiated sample at a similar dose and the same irradiation temperature (figure 3(b)). No strong modification of the Raman spectrum is noticed, which may suggest that Raman spectrum evolution is only due to radiation effects and not to chemical effects associated with the irradiation of Au ions into the SiC network. However, the detection limit of the Raman spectroscopy should be taken into account. Indeed, the maximum concentration in Au ions is around 10^{20} ions cm^{-3} (10^{16} ions cm^{-2} in a 1 μm thick layer), which roughly corresponds to 0.1% of Au ions into SiC. It corresponds to the detection limit for a micrometric laser spot.

4. Evolution of damage and disorder accumulation through Raman spectra analysis

4.1. Relative Raman intensity

In order to follow the damage accumulation, the relative Raman intensity (RRI) was determined and plotted versus the dose (figure 5). The RRI value corresponds to the average over the first-order Raman lines of the irradiated sample divided by the average intensity of the virgin sample [37]. As previously predicted in the literature [12, 37], the RRI decreases versus dose following an exponential law with a saturation at around 0.1 dpa. The loss of the Raman signal is mainly due to the increased optical absorption of the damaged layer consequently to the accumulation of absorbing centres [30, 34, 37]. For room temperature irradiation, saturation may correspond to the formation of a buried amorphous layer, by analogy with UV–visible spectroscopy [61]. The increase of the irradiation temperature leads to a lowering of the damage accumulation. The influence of the irradiation temperature on radiation effects was

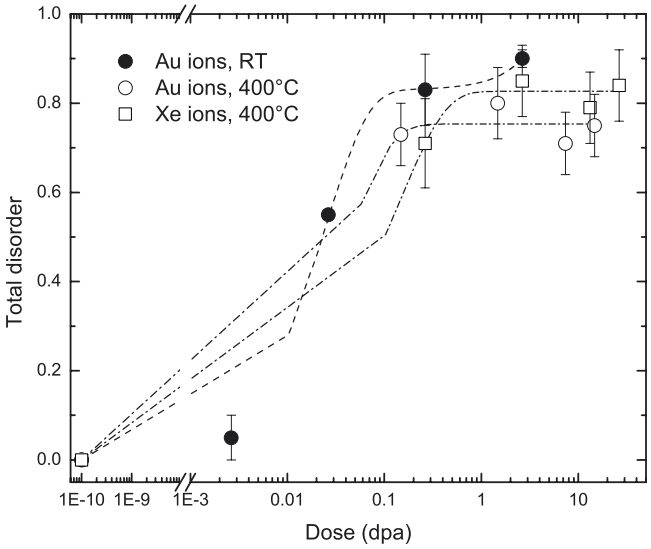

Figure 6. Total disorder determined for samples irradiated with Au ions at room temperature and 400 °C and with Xe ions at 400 °C. The dashed (for RT irradiation) and dash–dotted (for high irradiation temperature) curves correspond to the data fit with the direct impact/defect stimulated model (DI/DS) modified by Zhang *et al* [67].

intensively studied [12, 25] for SiC below 600 K. Simultaneous recovery of defects produced during irradiation may occur due to close-pair recombination and long-range migration of point defects.

No difference of the RRI saturated value is observed when the temperature of irradiation increases, despite the change of RRI saturation value with temperature reported by Heliou *et al* [37]. These authors observed an exponential law dependence between the RRI saturated value and the temperature of irradiation for Si-irradiated 6H-SiC. The discrepancy between our observations and the Heliou *et al* results may be explained by the importance of the recovery processes that strongly depend on the mass/energy of ions. Indeed, during irradiation, simultaneous damage recovery processes mitigate the production of radiation damage, and the rate of the damage evolution will depend on the relative magnitude of these two processes under irradiation conditions. Through the analysis of amorphization curves obtained for various ions, it was deduced that there is an increased efficiency of simultaneous damage recovery with decreasing particle mass. This behaviour was attributed to the effects of recoil spectra or to the increase in the electronic to nuclear stopping ratio [12, 13].

4.2. Total disorder

Menzel *et al* [36] defined the 1-A_{norm} value, which corresponds to the total area A under the principal first-order lines normalized to the value A^{cryst} of the crystalline material ($A_{\mathrm{norm}} = A/A^{\mathrm{cryst}}$). By comparison with the number of displaced atoms deduced from RBS/C spectra, they concluded on the representativeness of the 1-A_{norm} value for the total disorder. The total disorder was determined for Au- and Xe-ion irradiations at room temperature and 400 °C (figure 6).

The total disorder increases versus dose and saturates at around 0.264 dpa for room temperature irradiation. Saturation is associated with the formation of the buried amorphous layer in the irradiated zone, which is consistent with the corresponding Raman spectrum.

However, for a dose of 2.64 dpa, the irradiated zone is completely amorphous according to the shape of the resulting Raman spectrum, whereas the total disorder is lower than unity, the characteristic value for a totally disordered state. Consequently, amorphous SiC has a significant degree of ordering far from the maximum possible value [62–64]. EXAFS–EXELFS results clearly indicate that the amorphous phases are not formed of random arrangements of Si and C atoms but exhibit short-range order (SRO) at the level of the first coordination shell [65, 66].

The increase of irradiation temperature slows down the accumulation of disorder. Saturation results from the recovery processes enhanced by the rising of the irradiation temperature and the balance established between damage accumulation and simultaneous annealing. The effect of temperature on disorder is not as drastic as previously observed for the disorder deduced by RBS spectroscopy [23, 58]. No differences are observed between Au- and Xe-ion irradiations.

4.3. Chemical disorder

The state of damaged silicon carbide can be characterized by the standard order parameters, such as long-range order (LRO) and short-range order (SRO) parameters, which relate damage to the structure and chemical state of SiC. The LRO parameter refers to the degree of order with respect to the lattice sites, whereas the SRO parameter describes the degree of the chemical state with respect to the local arrangement of atoms, which can be partially preserved even when the LRO is completely lost. The homonuclear ratio R_{hnb}, defined for SiC as the ratio of the number of homonuclear bonds to twice the number of heteronuclear bonds, provides a full homonuclear analysis. Chemical disorder χ, defined as the ratio of the C–C bonds to C–Si bonds, is not a full homonuclear bond analysis and is specified only for C atoms. The χ value seems to be a quite good approximation [68] of R_{hnb}. The ratio ranges from zero for perfect short-range order to unity for random short-range disorder.

A rough determination of the χ parameter from Raman spectra is possible with the assumption that the intensity of the Raman peaks is proportional to the concentration of Si–C and C–C bonds. The TO-phonon line (766 cm^{-1}) was chosen as a reference for the Si–C bond concentration because it remains visible even in highly damaged samples. The peak located around 1420 cm^{-1} was used as a reference for the C–C bond. Nevertheless, the signal-to-noise ratio in the C–C vibration range is far from being negligible so the accuracy is limited and the results only give a tendency of the evolution of the chemical disorder.

The chemical disorder was estimated for α-SiC irradiated with Au ions at room temperature and at 400 °C and for a sample irradiated with Xe ions at 400 °C (figure 7). The chemical disorder increases with the dose and reaches a saturation step at around 2.5 dpa. Saturation may be attributed to amorphization for room temperature irradiation. The effect of temperature is to considerably decrease the chemical disorder and reduce its value at the saturation step. It is attributed to the recovery processes, which were enhanced by the increase of the irradiation temperature. No influence of ion species is noticed on the variations of the chemical disorder.

5. Discussion

5.1. Evolution of the structure

The structural evolution is in agreement with previous studies on irradiated SiC [30, 34, 35]. Indeed, the Raman spectrum of irradiated SiC generally presents several bands in the Si–Si, Si–C and C–C vibration domains and a clear decrease of the Raman line intensities (figures 2(a)

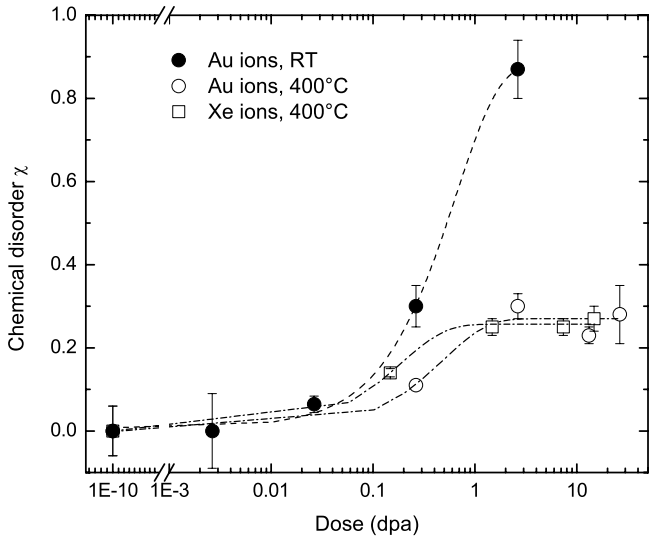

Figure 7. Chemical disorder determined for Au irradiations at room temperature and at 400 °C and for Xe irradiations at 400 °C. The dashed (for RT irradiation) and dash–dotted (for high irradiation temperature) curves correspond to the data fit with an exponential law.

and (b) and 3(a)). The principal effect shown by Raman spectroscopy is the formation of homonuclear bonds. However, the process is still not elucidated. For Si–Si bonds, it might consist in the replacement of the carbon atom, kicked out by the ion used for irradiation, by a silicon atom and vice versa. For the formation of C–C bonds, the proposed mechanism is based on the accumulation of interstitials or antisite carbon via condensation of C interstitials generated on the path of ions [69–71].

5.1.1. Structure of the disordered/distorted state. For low doses (0.026 dpa, RT), the Raman spectrum is composed of several bands related to Si–Si, Si–C and C–C vibrations in addition to the four first-order Raman lines characteristic of crystalline SiC (766, 780, 797 and 966 cm^{-1}). The Si–C bands, which are not related to crystalline SiC but to irradiated SiC, are spread over the 600–1000 cm^{-1} range. The appearance of these additional bands may be due to the lack of transitional invariance or long-range order. The Raman selection rules and wavevector conservation are no longer valid owing to the damage accumulation [35]. Furthermore, the formation of a disordered network structure associated with bond angle distortions may be evidenced [26] by the presence of bands around 500–600 cm^{-1}. In fact, the Raman spectrum is similar to that obtained by Bolse *et al* [26, 28] for low fluence. According to these authors, the overall sp^3 bond structure and the short-range order may be almost completely conserved, where each silicon atom is surrounded approximately by four C atoms and vice versa. These assumptions are supported by computer simulations, which predicted the formation of a distorted network provoked by the formation of homonuclear bonds [62, 63, 68].

In the domain of Si–Si vibrations, the bands at 200, 260 and 520 cm^{-1} are similar to the characteristic vibrations of crystalline silicon [47–49]. This may suggest a partial ordering of the Si–Si bonds in the SiC network. The band around 450 cm^{-1} may be relative to Si–O–Si vibrations [50] that may indicate the presence of SiO_2, probably located on the SiC surface. The identification of the Si–O band is however difficult due to the decrease of the Raman (Stokes) scattering efficiency with respect to crystalline Si [72, 73].

In the carbon vibration range, three bands are visible. One band is located around 1100 cm^{-1} in the sp^3-bonded domain of vibrations. The two bands at 1420 and 1540–1560 cm^{-1} are respectively the D and G bands characteristic of sp^2 carbon [50–56]. It should be noted that the identification of the 1400 cm^{-1} band with the D band is not the only possibility. The experiments on a-SiC_x films revealed that the D band disappears and the G band shifts down as the Si content increases [74]. The G band is issued from the *in-plane* C–C vibration whereas the D band is generally observed in disordered structures. The geometry for C–C bonds remains hypothetic in irradiated SiC, as C atoms can be both in planar or tetrahedral geometry. The band around 1400 cm^{-1} is in general associated with C sp^2 whereas the band at 1080 cm^{-1} is clearly in the range of C sp^3. Several interpretations can be envisaged to explain the appearance of a band around 1100 cm^{-1}. In pure carbon, the band is assigned to disordered sp^3-bonded carbon [75] or to the surface phonon mode of diamond [76]. In nano-crystallized silicon carbide, the band located at 1100 cm^{-1} is associated with sp^3 hybridization [51, 52]. Another explanation rises from the simulation of the G band. Indeed, the BWF line for the G peak accounts for residual Raman intensity at 1100 cm^{-1} where the Gaussian fit needs a supplementary peak. Thus, the band might not be related to a C–C vibration but rather to the tail of the G peak [56].

5.1.2. Structure of the amorphous state. The increase of the dose leads to a strong evolution of the structure. The evolution of the Raman spectra suggests a continuous transformation from the disordered/distorted state into the amorphous one. Numerous simulations supported by experimental data proposed that amorphous SiC is made of a chainlike structure of mixed sp^2/sp^3 C surrounded by Si–C and Si–Si networks, where Si gives rise to strongly distorted diamond-like sites [62–64, 77–80]. According to Finocchi *et al* [62], 40–45% of the bonds formed by C atoms are homonuclear. This description seems to be consistent with the Raman spectrum of an amorphous sample (2.64 dpa, RT).

The two bands situated at 200 and 500 cm^{-1} are related to Si–Si vibrations [34, 48, 52, 81]. Conservation of phonon momentum in crystalline silicon leads to a narrow optical mode at 520 cm^{-1}. In amorphous silicon, the q selection rules do not apply due to the loss of long-range order. All phonons are therefore optically allowed and the Raman spectrum resembles the phonon density of states with a broad band [82] at 480 cm^{-1}. In the case of irradiated SiC, the Si band shifts from 540 to 500 cm^{-1}, that may correspond to a randomization of the Si–Si bonds. The fact that the Si band does not reach the characteristic frequency of 480 cm^{-1} may be due to the coupling of Si atoms to the lighter carbon atoms into the SiC network [77]. The accommodation of the network to the substitution and the coupling may imply a distortion of the Si tetrahedrons as already observed through simulation [62] or experiments [80].

The broad band located at 800 cm^{-1} is composed of two sub-bands (766 and 870 cm^{-1}), which are attributed to amorphous or highly disordered SiC [30, 34, 80, 82]. By contrast, the bands observed for lower doses (600, 661, 920, 935 and 954 cm^{-1}) may be attributed to weakly disordered/distorted SiC. However this assignment must be confirmed by other results.

The broad band near 1430 cm^{-1} is attributed to the existence of amorphous C [30, 34, 57]. The fit of the C–C domains shows that only one band, close in frequency to the initial D band for lower dose, is needed. However, the signal-to-noise ratio prevents us from identifying a possible small contribution of the G band. In the literature, the band situated at 1430 cm^{-1} is interpreted as a signature of mixed sp^2 and sp^3 coordination in the SiC disordered network. This is confirmed by theoretical calculations [62, 79, 83] and structural studies [81, 84, 85] of a-Si–C:H. More precisely, Meneghini *et al* [85] observed that the C–C distance is in between those of diamond and graphite. This C–C bond length change is currently observed for irradiated carbon. In this material, a gradual transition from graphite-like spectra to diamond-like spectra

occurs owing the incorporation of four-coordinated atoms into the structure [86]. However, no strong evidence of sp^3 C in bulk diamond (1332 cm^{-1}, [87]) or in amorphous diamond (broad band near 1245 cm^{-1}, [88]) structure is noticed in the Raman spectrum of amorphous SiC.

5.2. Simulation of disorder accumulation

The dotted lines in figure 6 are least-square fits using the direct impact/defect stimulated model (DI/DS) modified by Zhang *et al* [67]. This model is generally used to reproduce the variations of the number of displaced atoms extracted from RBS data [12, 58, 89]. Recently, Zhang *et al* [67] included new terms relative to defects and defect cluster accumulation. The disorder S is given by the expression

$$S = f_a + S_d + S_c, \tag{1}$$

where f_a, S_d and S_c are respectively the contribution of irradiation-induced amorphization (f_a) (DI/DS model), irradiation-induced interstitials and small interstitial clusters in the residual crystalline regions (S_d), and extended defect clusters or precipitates formed at high temperatures (S_c).

The amorphous fraction, f_a, is given by the expression

$$f_a = 1 - (\sigma_a + \sigma_s)/(\sigma_s + \sigma_a \exp[(\sigma_a + \sigma_s) D]), \tag{2}$$

where σ_a is the amorphization cross-section, σ_s is the effective cross-section for defect-stimulated amorphization and D is the dose (dpa).

The contribution of the radiation defects to disorder S_d is expressed by the relation

$$S_d = S_d^* \left[1 - \exp(-B D)\right](1 - f_a), \tag{3}$$

where S_d^* is the saturation value for the defect-induced disorder, which is proportional to the local displacement rate and B (dpa^{-1}) is proportional to an effective recombination volume for the specific defect giving rise to S_d.

The relative disorder in the residual crystalline regions S_c is expressed as

$$S_c = S_c^* \left[1 - \exp(-R D)\right](1 - f_a), \tag{4}$$

where S_c^* is the saturation value of disorder due to the formation of irradiation-induced large clusters and R (dpa^{-1}) is proportional to an effective sink strength to form extended clusters.

This model was successfully used to simulate disorder for Al_2^{2+}- and Au^{2+}-irradiated SiC, especially for temperature close to the critical temperature of amorphization [58, 67]. It involves the fit of six different parameters, whereas only three curves are available. We used as starting values those given by Zhang *et al* [67]. The high number of fitting parameters with respect to the low number of data implies a high incertitude on parameter values. Therefore, we only extracted the more relevant parameters used by Zhang *et al*, which are the cross-section values (the probability for a process to occur). For the curve related to room temperature irradiation, the relevant parameters seem to be the amorphization cross-section σ_a and the effective cross-section for defect-stimulated amorphization σ_s that are equal to respectively 2 ± 0.5 and 20 ± 5 dpa^{-1}. For the irradiation at high temperature, the relevant parameters seem to be the effective sink strength to form extended clusters R, that is equal to 6 ± 1 and 20 ± 1 dpa^{-1} for Au and Xe irradiations respectively.

By contrast, the extended Avrami–Johnson–Mehl model modified by Carter [90] failed to reproduce the accumulation of disorder in SiC for high temperatures [91]. It seems that the DI/DS model is also adapted to fit the disorder data deduced from Raman spectra for irradiation at room temperature and at higher temperatures.

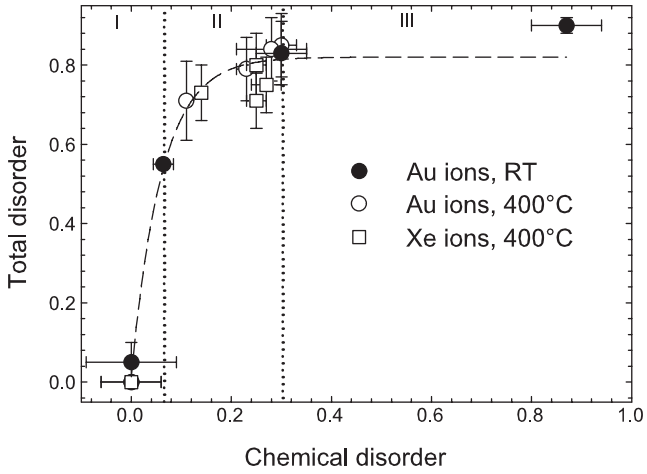

Figure 8. Variations of the total disorder with the chemical disorder induced by irradiations with Au ions at room temperature and at 400 °C and with Xe ions at 400 °C. Definition of the three stages I, II and III. The dashed curve corresponds to the data fit with an exponential law.

5.3. Correlation between total disorder and chemical disorder

In figure 8, the total disorder is plotted as a function of the chemical disorder. A clear correlation can be established between the two types of disorder. The resulting curve is divided into three stages. In the first stage (stage I), for $\chi < 0.1$, only the total disorder increases. In the second stage (stage II), for $0.1 < \chi < 0.3$, both total disorder and chemical disorder increase. In the third stage (stage III), for $\chi > 0.3$, the total disorder reaches a saturation level whereas the chemical disorder increases.

Each stage can be also associated with a specific Raman spectrum. In the first stage, the Raman spectrum is almost unchanged upon irradiation, total and chemical disorders are close to zero and the Raman line intensities are close to those of the virgin sample. In the second stage, the total disorder is high and the chemical disorder is in an intermediate value. Corresponding Raman spectra show several new bands related to the formation of homonuclear bonds and to the breakdown of the Raman selection rules induced by the accumulation of damage in the structure. In the third stage, the Raman spectrum is that expected for an amorphous SiC. The total and chemical disorders estimated from the spectrum are high.

The evolution of the Raman spectra and of the parameters of total and chemical disorder are consistent with the damage accumulation process proposed by Zhang *et al* [67] based on the fit of Si and C disorder curves with the DI/DS model. The first stage may be related to the formation of isolated defects. In the second stage, the disordering rate is enhanced and may be associated with defect-stimulated amorphization, that leads to the growth of amorphous nuclei and coalescence of amorphous domains. The third stage may correspond to the amorphization of the irradiated layer and the eventual formation of a continuous amorphous layer. In all the domains of disorder, the chemical disorder increases and seems to be the driving force of the amorphization in agreement with the Yuan and Hobbs assumption [68] on a chemical disorder threshold for amorphization.

6. Conclusions

Heavy-ion irradiation induces a decrease of the Raman line intensities related to crystalline SiC and the appearance of several new bands, Si–Si, Si–C and C–C. The new Si–C bands

were attributed to the breakdown of the Raman selection rules induced by the accumulation of damage. Si–Si and C–C vibrations give evidence of the formation of homonuclear bonds within the SiC network. The structure strongly changes with the increase of the dose. Several Si–C bands disappear and the bands become broader. For low doses, the overall sp^3 bond structure and the chemical order may be almost completely conserved. By contrast, the amorphous state shows a strong randomization of the Si–Si, Si–C and C–C bonds. Nevertheless, no strong evidence of sp^3 C vibrations is provided.

The relative Raman intensity (RRI) decreases exponentially with increasing dose because of the absorption of the irradiated layer. The total disorder follows a sigmoidal curve, which is well fitted by the direct impact/defect stimulated model. The chemical disorder expressed as the ratio of C–C bonds to Si–C bonds increases exponentially versus dose. A clear correlation is established between the total disorder and the chemical disorder, and three stages are defined according to the value of the chemical disorder, which seems to be the driving force of the amorphization process. The existence of a chemical disorder threshold around 30% is confirmed.

The increase of the irradiation temperature generates several effects on the structure and the disorder accumulation. The temperature rise allows the stabilization of a disordered/distorted state and induces a slowing down of the disorder production (total and chemical disorder) due to an enhancement of the dynamic annealing.

Acknowledgment

This work was followed and supported by the joint research program ISMIR between CEA and CNRS.

References

[1] Price R J 1973 *J. Nucl. Mater.* **48** 47–57
[2] Yano T, Miyazaki H, Akiyoshi M and Iseki T 1998 *J. Nucl. Mater.* **253** 78–86
[3] Senor D J, Youngblood G E, Greenwood L R, Archer D V, Alexander D L, Chen M C and Newsome G A 2003 *J. Nucl. Mater.* **317** 145–59
[4] Blackstone R and Voice E H 1971 *J. Nucl. Mater.* **39** 319–22
[5] Huang H and Ghoniem N 1997 *J. Nucl. Mater.* **250** 192–9
[6] Zinkle S J and Ghoniem N M 2000 *Fusion Eng. Des.* **51/52** 55–71
[7] Edmond J A, Withrow S P, Kong H S and Davis R F 1986 *Mater. Res. Soc. Proc.* **51** 395–402
[8] Heera V, Stoemenos J, Kögler R and Skorupa W 1995 *J. Appl. Phys.* **77** 2999–3009
[9] Beaufort M F, Pailloux F, Declémy A and Barbot J F 2003 *J. Appl. Phys.* **94** 7116–20
[10] Snead L L and Zinkle S J 1995 *Mater. Res. Soc. Proc.* **373** 377–82
[11] Zinkle S J and Snead L L 1996 *Nucl. Instrum. Methods Phys. Res.* B **116** 92–101
[12] Weber W J, Wang L M, Yu N and Hess N J 1998 *Mater. Sci. Eng.* A **253** 62–70
[13] Wendler E, Heft A and Wesch W 1998 *Nucl. Instrum. Methods Phys. Res.* B **141** 105–17
[14] Grisola J, de Mauduit B, Gimbert J, Billon Th, Ben Assayag G, Bourgerette C and Claverie A 1999 *Nucl. Instrum. Methods Phys. Res.* B **147** 62–7
[15] Heera V, Stoemenos J, Kögler R, Voelskow M and Skorupa W 1999 *J. Appl. Phys.* **85** 1378–86
[16] Persson P O A, Hultman L, Janson M S, Hallen A, Yakimova R, Pankin D and Skorupa W 2002 *J. Appl. Phys.* **92** 2501–5
[17] Heera V, Kögler R and Skorupa W 1995 *Appl. Phys. Lett.* **67** 1999–2001
[18] Heft A, Wendler E, Heindl J, Bachmann T, Glaser E, Strunk H P and Wesch W 1996 *Nucl. Instrum. Methods Phys. Res.* B **113** 239–43
[19] Pacaud Y, Stoemenos J, Brauer G, Yankov R A, Heera V, Voelskow M, Kogler R and Skorupa W 1996 *Nucl. Instrum. Methods Phys. Res.* B **120** 177–80
[20] Höfgen A, Heera V, Eicchorn F and Skorupa W 1998 *J. Appl. Phys.* **84** 4769–74
[21] Bus T, van Veen A, Shiryaev A, Fedorov A V, Schut H, Tichelaar F D and Sietsma J 2003 *Mater. Sci. Eng.* B **102** 269–76

[22] Heera V, Prokert F, Schell N, Seifarth H, Fukarek W, Voelskow M and Skorupa W 1997 *Appl. Phys. Lett.* **70** 3531–3
[23] Jiang W, Weber W J, Thevuthasan S and McCready D E 1999 *Surf. Interface Anal.* **27** 179–84
[24] Ohno T, Onose H, Sugawara Y, Asano K, Hayashi T and Yatsuo T 1999 *J. Electron. Mater.* **28** 180–5
[25] Jiang W, Weber W J, Zhang Y, Thevuthasan S and Sutthanandan V 2003 *Nucl. Instrum. Methods Phys. Res.* B **207** 92–9
[26] Bolse W, Conrad J, Rödle T and Weber T 1995 *Surf. Coat. Technol.* **74/75** 927–31
[27] Musumeci P, Calcagno L, Grimaldi M G and Foti G 1996 *Appl. Phys. Lett.* **69** 468–70
[28] Bolse W, Conrad J, Harbsmeier F, Borowski M and Rödle T 1997 *Mater. Sci. Forum* **248/249** 319–25
[29] Musumeci P, Reitano R, Calcagno L, Roccaforte F, Makhtari A and Grimaldi M G 1997 *Phil. Mag.* B **76** 323–33
[30] Bolse W 1998 *Nucl. Instrum. Methods Phys. Res.* B **141** 133–9
[31] Wendler E and Peiter G 2000 *J. Appl. Phys.* **87** 7679–84
[32] McHargue C J, Farlow G C, Begun G M, Williams J M, White C W, Appleton B R, Sklad P S and Angelini P 1986 *Nucl. Instrum. Methods Phys. Res.* **16** 212–20
[33] White C W, McHargue C J, Sklad P S, Boatner L A and Farlow G C 1989 *Mater. Sci. Rep.* **4** 41–146
[34] Pérez-Rodriguez A, Pacaud Y, Calvo-Barrio L, Serre C, Skorupa W and Morante J R 1996 *J. Electron. Mater.* **25** 541–7
[35] Hobert H, Dunken H, Menzel R, Bachmann T and Wesch W 1997 *J. Non-Cryst. Solids* **220** 187–94
[36] Menzel R, Gärtner K, Wesch W and Hobert H 2000 *J. Appl. Phys.* **88** 5658–61
[37] Héliou R, Brebner J L and Roorda S 2001 *Nucl. Instrum. Methods Phys. Res.* B **175–177** 268–73
[38] Ziegler F, Biersack J P and Littmarck U 1985 *The Stopping and Range of Ions in Solids* (New York: Pergamon)
[39] Devanathan R and Weber W J 2000 *J. Nucl. Mater.* **278** 258–65
[40] McCulloch D G, Prawer S and Hoffman A 1994 *Phys. Rev.* B **50** 5905–17
[41] McCulloch D G and Prawer S 1995 *J. Appl. Phys.* **78** 3040–7
[42] Prawer S, Nugent K W and Jamieson D N 1998 *Diamond Relat. Mater.* **7** 106–10
[43] Feldman D W, Parker J H Jr, Choyke W J and Patrick L 1968 *Phys. Rev.* **170** 698–704
[44] Burton J C, Sun L, Pophristic M, Lukacs S J, Long F H, Feng Z C and Ferguson I T 1998 *J. Appl. Phys.* **84** 6268–73
[45] Burton J C, Sun L, Long F H, Feng Z C and Ferguson I T 1999 *Phys. Rev.* B **59** 7282–4
[46] Nakashima S and Harima H 1997 *Phys. Status Solidi* a **162** 39–64
[47] Lannin J S, Pilione L J, Kshirsagar S T, Messier R and Ross R C 1982 *Phys. Rev.* B **26** 3506–9
[48] Zwick A and Carles R 1993 *Phys. Rev.* B **48** 6024–32
[49] Ehbrecht M, Ferkel H, Huisken F, Holz L, Polivanov Yu N, Smirnov V V, Stelmakh O M and Schmidt R 1995 *J. Appl. Phys.* **78** 5302–6
[50] Mélinon P, Blase X, Kéghélian P, Perez A, Ray C, Pellarin M and Broyer M 2002 *Phys. Rev.* B **65** 125321
[51] Shroder R E, Nemanich R J and Glass J T 1990 *Phys. Rev.* B **41** 3738–45
[52] Mélinon P, Kéghélian P, Perez A, Ray C, Lermé J, Pellarin M, Broyer M, Boudeulle M, Champagnon B and Rousset J L 1998 *Phys. Rev.* B **58** 16481–90
[53] Tuinstra F and Koening J L 1970 *J. Chem. Phys.* **53** 1126–30
[54] Gilkes K W R, Sand H S, Batchelder D N, Robertson J and Milne W I 1997 *Appl. Phys. Lett.* **70** 1980–2
[55] Merkulov V I, Lannin J S, Munro C H, Asher S A, Veerasamy V S and Milne W I 1997 *Phys. Rev. Lett.* **78** 4869–72
[56] Ferrari A C and Robertson J 2000 *Phys. Rev.* B **61** 14095–107
[57] Compagnini G and Foti G 1997 *Nucl. Instrum. Methods Phys. Res.* B **127/128** 639–42
[58] Jiang W, Zhang Y and Weber W J 2004 *Phys. Rev.* B **70** 165208
[59] Williams P M, Mason P W and Watkins G D 1996 *Phys. Rev.* B **53** 12570–3
[60] Scheerer O, Juda U and Höhne M 1998 *Phys. Rev.* B **57** 9657–62
[61] Musmeci P, Calcagno L, Grimaldi M G and Foti G 1996 *Nucl. Instrum. Methods Phys. Res.* B **116** 327–31
[62] Finocchi F, Galli G, Parrinello M and Bertoni C M 1992 *Phys. Rev. Lett.* **68** 3044–7
[63] Kelires M 1992 *Phys. Rev.* B **46** 10048–60
[64] Tersoff J 1994 *Phys. Rev.* B **49** 16349–52
[65] Kaloyeros A E, Rizk R B and Woodhouse J B 1988 *Phys. Rev.* B **38** 13099–106
[66] Pascarelli S, Boscherini F, Mobilio S and Evangelisti F 1992 *Phys. Rev.* B **45** 1650–4
[67] Zhang Y, Weber W J, Jiang W, Wang C M and Shutthanandan V 2004 *J. Appl. Phys.* **95** 4012–8
[68] Yuan X and Hobbs L W 2002 *Nucl. Instrum. Methods Phys. Res.* B **191** 74–82
[69] Rahn L A, Colwell P J and Choyke W J 1976 *Proc. 3rd Int. Conf. on Light Scattering in Solids* ed M Balkanski, R C C Leite and S P S Porto (Paris: Flammarion) p 607
[70] Gali A, Deak P, Ordejon P, Son N T, Janzen E and Choyke W J 2003 *Phys. Rev.* B **68** 125201

[71] Mattausch A, Bockstedte M and Pankratov O 2004 *Phys. Rev.* B **70** 235211
[72] Kurcirkova A, Navratil K, Pajasova L and Vorlicek V 1996 *Appl. Phys.* A **63** 495–503
[73] Cardona M 1982 *Light Scattering in Solids II* (*Springer Topics in Applied Physics* vol 50) ed M Cardona and G Güntherodt (Berlin: Springer) pp 93–4
[74] Kulikovsky V, Vorlıcek V, Bohac P, Kurdyumov A and Jastrabık L 2004 *Diamond Relat. Mater.* **13** 1350–5
[75] Nemanich R J, Glass J T, Lucovsky G and Shroder R E 1988 *J. Vac. Sci. Technol.* A **6** 1783
[76] Prawer S, Nugent K W, Jamieson D N, Orwa J O, Bursill L A and Peng J L 2000 *Chem. Phys. Lett.* **332** 93–7
[77] Gorman M and Solin S A 1974 *Solid State Commun.* **15** 761–5
[78] Mui K, Basa D K, Smith F W and Corderman R 1987 *Phys. Rev.* B **35** 8089–102
[79] Chaihadar A, Carles R, Zwick A, Meunier C, Cros B and Durand J 1994 *J. Non-Cryst. Solids* **169** 37–46
[80] Musumeci P, Roccaforte F and Reitano R 2001 *Europhys. Lett.* **55** 674–8
[81] Serre C, Calco-Barrio L, Pérez-Rodriguez A, Romano-Rodriguez A, Morant J R, Pacaud Y, Kögler R, Heera V and Skorupa W 1996 *J. Appl. Phys.* **79** 6907–13
[82] Mishra P and Jain K P 2002 *Mater. Sci. Eng.* B **95** 202–13
[83] Gao F and Weber W J 2001 *J. Appl. Phys.* **89** 4275–81
[84] Petrich M A, Gleason K K and Reimer J A 1987 *Phys. Rev.* B **36** 9722–31
[85] Meneghini C, Pascarelli S, Boscherini F, Mobilio S and Evangelisti F 1991 *J. Non-Cryst. Solids* **137/138** 75–8
[86] Beeman D, Silverman J, Lynds R and Anderson M R 1984 *Phys. Rev.* B **30** 870–5
[87] Knight D S and White W B 1989 *J. Mater. Res.* **4** 385
[88] Orwa J O, Nugent K W, Jamieson D N and Prawer S 2000 *Phys. Rev.* B **62** 5461–71
[89] Weber W J, Jiang W and Thevuthasan S 2001 *Nucl. Instrum. Methods Phys. Res.* B **175–177** 26–30
[90] Carter G 1996 *J. Appl. Phys.* **79** 8285–9
[91] Henkel T, Heera V, Kögler R and Skorupa W 1998 *J. Appl. Phys.* **84** 3090–7